INTERNATIONAL JOURNAL FOR NUMERICAL METHODS IN FLUIDS, VOL. 20, 969–987 (1995)

COUPLED HEAT, WATER AND GAS FLOW IN DEFORMABLE POROUS MEDIA

DARIUSZ GAWIN

Department of Building Physics and Building Materials, Technical University of Lodz, Al. Politechniki 6, 93-590 Lodz, Poland

PAOLO BAGGIO

Istituto di Fisica Tecnica, Università di Padova, Via Marzolo 9, I-35131 Padova, Italy

AND

BERNHARD A. SCHREFLER*

Istituto di Scienza e Tecnica delle Costruzioni, Università di Padova, Via Marzolo 9, I-35131 Padova, Italy

SUMMARY

A fully coupled numerical model to simulate the slow transient phenomena involving heat and mass transfer in deforming porous media is developed. It makes use of the modified effective stress concept together with the capillary pressure relationship. The heat transfer through conduction and convection as well as the latent heat transfer (evaporation and/or condensation) is taken into account.

The governing equations in terms of displacements, temperature, capillary pressure and gas pressure are coupled non-linear differential equations and are solved by the finite element method.

The model is validated with respect to a documented experiment on semisaturated soil behaviour. Two other examples involving subsidence due to pumping from a phreatic aquifer and thermoelastic consolidation of saturated and semisaturated media are also presented.

KEY WORDS coupled heat and mass transfer; deforming porous media; phase change; mathematical model; numerical solution

1. INTRODUCTION

A fully coupled numerical model to simulate slow transient phenomena involving flow of heat, water and gas in deforming porous media is presented. This model is aimed at handling situations which span from fully saturated to almost dry conditions.

The mathematical model consists of balance equations of mass, linear momentum and energy and of the appropriate constitutive equations. The balance equations are first written at the microscopic level for each constituent and then macroscopic balance equations are obtained by systematic application of averaging theories based on spatial averaging operators.[1–10]

Particular aspects of the model are the following. The gas phase is considered to be an ideal gas composed of dry air and vapour, which are regarded as two miscible species. Furthermore, phase change is taken into account as well as heat transfer through conduction and convection and latent heat

* Author to whom correspondence should be addressed.

CCC 0271–2091/95/090969–19

transfer (evaporation–condensation). This model is an extension of the heat and mass transfer formulation of Baggio *et al.*,[11,12] based on Whitaker's approach,[9,10] to the case of deformable porous media. It is a step forward when compared with a previous model[13] where latent heat transfer and phase change were neglected. The differences in behaviour due to these two factors are significant in simulations where the conditions are such that these phenomena may develop (e.g. long time spans or/and high temperature gradients). The model makes further use of a modified effective stress concept together with the capillary pressure relationship.

The above-mentioned balance equations, after introduction of the constitutive relationships, are discretized in space by means of the finite element method and in time by finite differences. The chosen macroscopic primary variables are displacements, capillary pressure, gas pressure and temperature. These correspond to real measurable quantities directly linked to laboratory practice, which is an important aspect when selecting the appropriate constitutive equations.

As far as other published solutions including solid matrix deformation are concerned, only a few can be found in the literature. Most models address the case of a rigid matrix.[1,14–16] The case of matrix deformation was dealt with in the already-mentioned model,[13] by Geraminegad and Saxena[17] and by Lewis *et al.*[18] In Reference 17 a modified version of the theory of Philip and de Vries[19,20] was applied in the heat transfer equation and the model incorporated only volumetric soil deformation. In Reference 18 geothermal reservoirs were considered above the critical temperature, so that capillary pressure effects could be neglected and a unique continuity equation for both steam and water could be used.

In this paper the governing equations are briefly derived and the discretized equations shown, which are then solved by a Newton-type procedure. Three examples are solved which were used for the validation of the code based on the outlined approach. The last example clearly shows the need for a complete model which includes also phase change and latent heat.

2. CONSTITUTIVE EQUATIONS

The semisaturated porous medium is modelled as multiphase system where the voids of the skeleton are filled partly with liquid water and partly with gas assumed to behave as an ideal mixture of dry air and water vapour. The state of the medium is described by gas pressure p_g, capillary pressure p_c, temperature T and the displacement vector of the solid matrix, $\mathbf{u}$.

The saturation of liquid water, S, is an experimentally determined function of capillary pressure p_c and temperature T, i.e.

$$S = S(p_c,\ T), \tag{1}$$

while its pressure p_l can be expressed as

$$p_l = p_g - p_c. \tag{2}$$

The equation of state of perfect gases applied to dry air (ga), vapour (gw) and moist air (g) gives

$$p_{ga} = \rho_{ga} TR/M_a, \qquad p_{gw} = \rho_{gw} TR/M_w, \qquad p_g = p_{ga} + p_{gw}, \qquad \rho_g = \rho_{ga} + \rho_{gw}. \tag{3}$$

Owing to the curvature of the meniscus separating the liquid (water) phase from the gas phase inside the pores of the medium (considered as a capillary porous body), the equilibrium vapour pressure can be obtained from the Kelvin relationship. This gives the relative humidity (RH) of the moist air inside the pores as

$$\mathrm{RH} = \frac{p_{gw}}{p_{gws}} = \exp\left(-\frac{p_c M_w}{\rho_l RT}\right), \tag{4}$$

where the water vapour saturation pressure p_{gws}, which depends only upon temperature T, can be obtained from the Clausius–Clapeyron equation or from empirical correlations such as the one proposed by Hyland and Wexler.[21]

The constitutive laws of the solid phase are introduced through the concept of modified effective stress

$$\sigma'' = \sigma + \alpha p \mathbf{I}, \tag{5}$$

where σ is the total stress tensor, $\mathbf{I}$ is the unit tensor, α is the Biot constant and p is the average pressure of the mixture of fluids surrounding the grains, which can be evaluated in the case of immiscible two-phase flow, using the averaging technique developed by Whitaker,[9,10,22] as

$$p = S \cdot p_l + (1 - S) \cdot p_g. \tag{6}$$

The Biot constant is introduced to account for the volumetric deformability of the particles and was shown[23–25] to be

$$\alpha = 1 - \frac{K_T}{K_S} \leq 1, \tag{7}$$

where K_T and K_S are the bulk moduli of the porous medium and the solid phase respectively.

For a discussion about the validity of the effective stress concept the interested reader is referred to Reference 26.

The constitutive relationship for the solid skeleton has the form

$$d\sigma'' = \mathbf{D}\left(d\varepsilon - d\varepsilon^T - d\varepsilon^0\right) \tag{8}$$

where $\mathbf{D}$ is the tangent matrix, $d\varepsilon^T = \mathbf{I}(\beta_s/3)dT$ is the strain increment caused by thermoelastic expansion, β_s is the cubic thermal expansion coefficient of the solid and $d\varepsilon^0$ represents the autogenous stain increments and the irreversible part of the thermal strains.[27]

3. GOVERNING EQUATIONS

In the following, only slow phenomena and small displacements are considered. Thermal equilibrium between solid matrix, gas and liquid is assumed, so the temperature is the same for the three constituents.

The formulation of heat and mass transfer in porous media is obtained starting from the appropriate local equations expressing the laws of continuum physics (see e.g. Reference 28), specifically the continuity equation for each species considered, the Navier–Stokes equation for quasi-steady creeping flow (i.e. with the time-dependent and convective terms neglected) and the energy equation (enthalpy balance) with viscous dissipation and reversible work neglected. In general such equations cannot be solved because of the complex geometry of the porous media, but using the volume-averaging technique,[1–3,9] we can obtain equations averaged on a *representative elementary volume* (REV)[1] of the porous medium.

The multiphase Darcy equation applied to the liquid phase and to the gas phase respectively gives

$$\mathbf{v}_l = -\frac{KK_{rl}}{\mu_l}\left(\nabla p_g - \nabla p_c - \rho_l \mathbf{b}\right), \tag{9}$$

$$\mathbf{v}_g = -\frac{KK_{rg}}{\mu_g}\left(\nabla p_g - \rho_g \mathbf{b}\right), \tag{10}$$

where $\mathbf{v}_l$ and $\mathbf{v}_g$ are the velocities of liquid and gaseous phase relative to the solid phase respectively and the vector $\mathbf{b}$ indicates the specific body force term (normally corresponding to the acceleration due to gravity). Usually in the gas phase the body force term $\rho_g \mathbf{b}$ is negligible.

Fick's law gives the relative average velocities of the diffusing species (dry air and water vapour) as

$$\mathbf{v}_{ga}^d = -\frac{M_a M_w}{M^2} D_{eff} \nabla\left(\frac{p_{ga}}{p_g}\right) = \frac{M_a M_w}{M^2} D_{eff} \nabla\left(\frac{p_{gw}}{p_g}\right) = -\mathbf{v}_{gw}^d, \tag{11}$$

$$\mathbf{v}_{gw}^d = -\frac{M_a M_w}{M^2} D_{eff} \nabla\left(\frac{p_{gw}}{p_g}\right). \tag{12}$$

The governing equations cast in conservation form can be written as follows:[9,27]
dry air conservation equation

$$\phi \frac{\partial}{\partial t}\left[(1-S)\rho_{ga}\right] + \alpha(1-S)\rho_{ga}\frac{\partial}{\partial t}(\nabla\cdot\mathbf{u}) + \nabla\cdot\left(\rho_{ga}\mathbf{v}_g\right) + \nabla\cdot\left(\rho_g \mathbf{v}_{gw}^d\right) = 0, \tag{13}$$

water species (liquid–vapour) conservation equation

$$\begin{aligned} &\phi \frac{\partial}{\partial t}\left[(1-S)\rho_{gw}\right] + \alpha(1-S)\rho_{gw}\frac{\partial}{\partial t}(\nabla\cdot\mathbf{u}) + \nabla\cdot\left(\rho_{gw}\mathbf{v}_g\right) - \nabla\cdot\left(\rho_g \mathbf{v}_{gw}^d\right) \\ &\quad = -\phi\rho_l\frac{\partial S}{\partial t} - \alpha S\rho_l\frac{\partial}{\partial t}(\nabla\cdot\mathbf{u}) + \nabla\cdot(\rho_l\mathbf{v}_l) \end{aligned} \tag{14}$$

energy conservation (enthalpy balance)

$$\begin{aligned} &\rho C_p\frac{\partial T}{\partial t} + (C_{pw}\rho_w\mathbf{v}_l + C_{pg}\rho_{gw}\mathbf{v}_g)\cdot\nabla T - \nabla\cdot(\lambda_{eff}\nabla T) \\ &\quad = \Delta h_{vap}\left(\phi\rho_l\frac{\partial S}{\partial t} + \alpha S\rho_l\frac{\partial}{\partial t}(\nabla\cdot\mathbf{u}) - \nabla\cdot(\rho_l\mathbf{v}_l)\right); \end{aligned} \tag{15}$$

the *linear momentum balance equation* for the whole mixture, neglecting inertial effects, can be written in terms of total stresses as[29–31]

$$\nabla\cdot\sigma + \rho\mathbf{b} = 0, \tag{16}$$

where ρ is the average density of the mixture,

$$\rho = (1-\phi)\rho_s + \phi S\rho_l + \phi(1-S)\rho_g, \tag{17}$$

ϕ is the porosity, ρ_s is the density of the solid, ρ_l is the density of the liquid water and ρ_g is the density of the gas.

It is further necessary to define the initial and boundary conditions. The initial conditions specify the full fields of gas pressure, capillary pressure, temperature and displacement:

$$p_g = p_g^0, \quad p_c = p_c^0, \quad T = T^0 \quad \text{and} \quad \mathbf{u} = \mathbf{u}^0 \quad \text{at } t = 0. \tag{18}$$

The boundary conditions can be imposed values on Γ_i or fluxes on Γ_i^q, where the boundary $\Gamma = \Gamma_i \cup \Gamma_i^q$. The imposed values on the boundary for gas pressure, capillary pressure, temperature and displacements are

$$p_g = \hat{p}_g \quad \text{on } \Gamma_g, \qquad p_c = \hat{p}_c \quad \text{on } \Gamma_c, \qquad T = \hat{T} \quad \text{on } \Gamma_T, \qquad \mathbf{u} = \hat{\mathbf{u}} \quad \text{on } \Gamma_u. \tag{19}$$

The volume-averaged flux boundary conditions for the water species and dry air conservation equations and for the energy equation to be imposed at the interface between the porous medium and the surrounding fluid are

$$\begin{aligned}
\left(\rho_{ga}\mathbf{v}_g + \rho_g \mathbf{v}_{gw}^d\right) \cdot \mathbf{n} &= q_{ga} \quad \text{on } \Gamma_g^q, \\
\left(\rho_{gw}\mathbf{v}_g + \rho_l \mathbf{v}_l - \rho_g \mathbf{v}_{gw}^d\right) \cdot \mathbf{n} &= \beta_c\left(\rho_{gw} - \rho_{gw\infty}\right) + q_{gw} + q_l \quad \text{on } \Gamma_c^q, \\
-\left(\rho_l \mathbf{v}_l \Delta h_{vap} - \lambda_{eff}\nabla T\right) \cdot \mathbf{n} &= \alpha_c(T - T_\infty) + q_T \quad \text{on } \Gamma_T^q,
\end{aligned} \tag{20}$$

where $\mathbf{n}$ is the unit vector, perpendicular to the surface of the porous medium, pointing towards the surrounding gas, $\rho_{gw\infty}$ and T_∞ are the mass concentration of water vapour and the temperature in the undisturbed gas phase far from the interface respectively, α_c and β_c are the convective heat and mass transfer coefficients respectively and q_{ga}, q_{gw}, q_l and q_T are the imposed dry air flux, the imposed vapour flux, the imposed liquid flux and the imposed heat flux respectively.

Equations (20) are the natural boundary conditions for the dry air equation (13), the water species conservation equation (14) and the energy conservation equation (15) respectively, when the solution of these equations is obtained through a weak formulation of the problem, as is usually done with the finite element method.[32]

The traction boundary conditions for the displacement field are

$$\sigma \cdot \mathbf{n} = \mathbf{t} \quad \text{on } \Gamma_u^q, \tag{21}$$

where $\mathbf{t}$ is the imposed traction.

4. DISCRETIZATION AND SOLUTION

Discretization of the governing equations is carried out by means of finite elements in space and finite differences in time. The notations of Zienkiewicz and Taylor[32] are used in the following, together with vector notation. The unknown variables are expressed in terms of their nodal values as

$$p_g = p_g(t) = \mathbf{N}_p \bar{\mathbf{p}}_g(t), \quad p_c = p_c(t) = \mathbf{N}_p \bar{\mathbf{p}}_c(t), \quad T = T(t) = \mathbf{N}_t \bar{\mathbf{T}}(t), \quad \mathbf{u} = \mathbf{u}(t) = \mathbf{N}_u \bar{\mathbf{u}}(t). \tag{22}$$

The integral or weak forms of the heat and mass transfer equations obtained following the Galerkin procedure and with the usual choice of shape functions N can be expressed in matrix form as

$$\begin{aligned}
\mathbf{C}_{gg}\dot{\bar{\mathbf{p}}}_g + \mathbf{C}_{gc}\dot{\bar{\mathbf{p}}}_c + \mathbf{C}_{gt}\dot{\bar{\mathbf{T}}} + \mathbf{C}_{gu}\dot{\bar{\mathbf{u}}} + \mathbf{K}_{gg}\bar{\mathbf{p}}_g + \mathbf{K}_{gc}\bar{\mathbf{p}}_c + \mathbf{K}_{gt}\bar{\mathbf{T}} + \mathbf{f}_g &= \mathbf{0}, \\
\mathbf{C}_{c}\dot{\bar{\mathbf{p}}}_g + \mathbf{C}_{cc}\dot{\bar{\mathbf{p}}}_c + \mathbf{C}_{ct}\dot{\bar{\mathbf{T}}} + \mathbf{C}_{cu}\dot{\bar{\mathbf{u}}} + \mathbf{K}_{cg}\bar{\mathbf{p}}_g + \mathbf{K}_{cc}\bar{\mathbf{p}}_c + \mathbf{K}_{ct}\bar{\mathbf{T}} + \mathbf{f}_c &= \mathbf{0}, \\
\mathbf{C}_{tg}\dot{\bar{\mathbf{p}}}_g + \mathbf{C}_{tc}\dot{\bar{\mathbf{p}}}_c + \mathbf{C}_{tt}\dot{\bar{\mathbf{T}}} + \mathbf{C}_{tu}\dot{\bar{\mathbf{u}}} + \mathbf{K}_{tg}\bar{\mathbf{p}}_g + \mathbf{K}_{tc}\bar{\mathbf{p}}_c + \mathbf{K}_{tt}\bar{\mathbf{T}} + \mathbf{f}_t &= 0,
\end{aligned} \tag{23}$$

where all the matrices are as listed in Appendix I.

Using the principle of virtual work and taking into account the boundary condition (21), the linear momentum balance equation (16) can be written in a weak form as:[27]

$$-\int_\Omega \delta\varepsilon^T \sigma \, d\Omega + \int_\Omega \rho \, \delta\mathbf{u}^T \mathbf{b} \, d\Omega + \int_\Gamma \delta\mathbf{u}^T \mathbf{t} \, d\Gamma = 0. \tag{24}$$

Application of (2), (6), the effective stress relationship (5) and the definition of the strain matrix relating strain and displacement, i.e.

$$\varepsilon = \mathbf{B}\mathbf{u}, \tag{25}$$

allows us to express (24) in matrix form as

$$-\int_{\Omega} \mathbf{B}^{\mathrm{T}}\sigma \, \mathrm{d}\Omega + \mathbf{K}_{\mathrm{ug}}\bar{\mathbf{p}}_{\mathrm{g}} + \mathbf{K}_{\mathrm{uc}}\bar{\mathbf{p}}_{\mathrm{c}} + \mathbf{K}_{\mathrm{ut}}\bar{\mathbf{T}} + \mathbf{f}_{\mathrm{u}} = 0, \tag{26}$$

where $\mathbf{f}_{\mathrm{u}}$ and the coupling matrices $\mathbf{K}_{\mathrm{ug}}$, $\mathbf{K}_{\mathrm{uc}}$ and $\mathbf{K}_{\mathrm{ut}}$ are as listed in Appendix I.

The effective stresses are obtained from integration of (8), starting from the known initial values of the problem.

Semidiscretization of the conservation equations (and of the other ones required to complete the model) with the standard Galerkin method (weighted residuals)[32] and the principle of virtual work[27] results in a non-symmetric, non-linear and coupled system of ordinary differential equations of the form

$$\mathbf{C}(\mathbf{x})\dot{\mathbf{x}} + \mathbf{K}(\mathbf{x})\mathbf{x} + \mathbf{f}(\mathbf{x}) = 0, \tag{27}$$

where

$$\mathbf{x} = \begin{Bmatrix} \bar{\mathbf{p}}_{\mathrm{g}} \\ \bar{\mathbf{p}}_{\mathrm{c}} \\ \bar{\mathbf{T}} \\ \bar{\mathbf{u}} \end{Bmatrix} \tag{28}$$

and the non-linear (matrix) coefficients $\mathbf{C}(\mathbf{x})$, $\mathbf{K}(\mathbf{x})$ and $\mathbf{f}(\mathbf{x})$ are obtained by assembling the submatrices indicated in (23) and (26). Time discretization is accomplished through a fully implicit finite difference scheme (backward difference):[32]

$$\mathbf{C}(\mathbf{x}_{n+1})\frac{\mathbf{x}_{n+1} - \mathbf{x}_n}{\Delta t} + \mathbf{K}(\mathbf{x}_{n+1})\mathbf{x}_{n+1} + \mathbf{f}(\mathbf{x}_{n+1}) = 0, \tag{29}$$

where n is the time step number and Δt is the time step.

Considering the non-linearity of the system of equations (17), the solution is obtained with a Newton–Raphson-type procedure

$$\begin{aligned} \frac{1}{\Delta t}\left(\frac{\partial}{\partial \mathbf{x}}\mathbf{C}(\mathbf{x}^l_{n+1})(\mathbf{x}^l_{n+1} - \mathbf{x}_n) + \mathbf{C}(\mathbf{x}^l_{n+1})\right)\Delta\mathbf{x}^l_{n+1} \\ + \left(\frac{\partial}{\partial \mathbf{x}}\mathbf{K}(\mathbf{x}^l_{n+1})\mathbf{x}^l_{n+1} + \mathbf{K}(\mathbf{x}^l_{n+1}) + \frac{\partial}{\partial \mathbf{x}}\mathbf{f}(\mathbf{x}^l_{n+1})\right)\Delta\mathbf{x}^l_{n+1} \\ = -\left(\mathbf{C}(\mathbf{x}^l_{n+1})\frac{\mathbf{x}^l_{n+1} - \mathbf{x}_n}{\Delta t} + \mathbf{K}(\mathbf{x}^l_{n+1})\mathbf{x}_{n+1} + \mathbf{f}(\mathbf{x}^l_{n+1})\right), \end{aligned}$$

where l is the iteration index and at the end of each iteration the primary variables are updated as

$$\mathbf{x}^{l+1}_{n+1} = \mathbf{x}^l_{n+1} + \Delta\mathbf{x}^l_{n+1}. \tag{31}$$

A problem arises when the medium is fully saturated, because in this case the gas pressure p_{g} and the capillary pressure p_{c} have no physical meaning, while on the other hand the state of the liquid water in the medium is described by two variables (since in such a situation there are only two degrees of freedom on top of solid displacements: liquid pressure p_{l} and temperature T). The problem is treated with a formal modification of the relationship between saturation S and capillary pressure p_{c}: when the saturation S becomes equal to one, the sign of the capillary pressure is set negative and the value equal to the pressure in the liquid above gas pressure.

The fully saturated state is detected by monitoring the sign of the capillary pressure p_{c}: when

such a condition is reached, the *dry air conservation equation* is dropped and the gas pressure p_g is set equal to atmospheric pressure ('switching' from partially saturated to fully saturated state equations or vice versa). In practice, capillary and gas pressure oscillations usually arise when this switch is performed, so it is necessary to apply this procedure for slightly lower saturation value $S < 1$ (capillary pressure $p_c > 0$) which depends on the shape of the saturation–capillary pressure relationship and on the problem analysed. These oscillations are possibly due to the sudden switch of element behaviour (there is a change in governing equations) in a part of the domain, which in turn causes different convergences to solution in fully and partially saturated zones of the domain and produces oscillations in the Newton iteration procedure.[33] Another possible reason is the occurrence of an incompressible–undrained limit which may cause spurious pressure oscillations.[32]

Based on the presented discretization, the HMTRA-DEF research computer code has been developed for solution of the non-linear and non-symmetrical system of equations governing heat and mass transfer in a deforming porous medium.

5. NUMERICAL EXAMPLES

It is very difficult to choose appropriate tests to validate the proposed model because of the lack of any analytical solutions for this type of coupled problem, where deformations of the solid skeleton are studied together with the saturated–unsaturated flow of mass and heat transfer. There are also very few documented laboratory experiments. One of these is the experiment conducted by Liakopoulos[34] on the isothermal drainage of water from a vertical column of sand. This test was also used by Narasimhan and Witherspoon,[35] Schrefler and Simoni,[36] Zienkiewicz *et al.*[25] and Schrefler and Zhan[26] to check their numerical models. Then two other examples relating respectively to subsidence due to pumping from a phreatic aquifer[37,38] and thermoelastic consolidation[13,27] for fully and partially saturated conditions are solved.

In all these examples isoparametric Lagrangian elements are used, the same for the pressure, temperature and displacement fields. Furthermore, linear elastic material behaviour and the Biot constant $\alpha = 1$ are assumed.

5.1. *Drainage test*

In the experiment of Liakopoulos[34] a column of Perspex 1 m high was packed with Del Monte sand and instrumented to measure continuously the moisture tension at several points along the column. Before the start of the experiment ($t < 0$) water was added continuously from the top and was allowed to drain freely at the bottom through a filter until uniform flow conditions were established. At $t = 0$ the water supply was ceased and the tensiometer readings were recorded. The porosity, $\phi = 29{\cdot}75\%$, and hydraulic properties of Del Monte sand were measured by Liakopoulos in an independent set of experiments.[26,34] For numerical purposes the column was simulated by 10 and 20 four-, eight- and nine-node isoparametric finite elements of equal size and different meshes in the time domain were used, giving practically the same results. At the beginning, besides the uniform flow conditions (i.e. unit vertical gradient of the potential and $p_c = 0$ on the top surface), a mechanical equilibrium state was assumed. The boundary conditions were the following: for the lateral surface, $q_T = 0$, $u_h = 0$, where u_h is the horizontal displacement of soil; for the top surface, $p_g = p_{atm}$, where p_{atm} is atmospheric pressure, $T = 293{\cdot}15$ K; for the bottom surface, $p_g = p_{atm}$, $p_c = 0$ for $t > 150$ s, while the water pressure p_l was assumed to change linearly from the initial value to zero for $t < 150$ s, $T = 293{\cdot}15$ K, $u_h = u_v = 0$, where u_v is the vertical displacement of soil.

Liakopoulos did not measure the mechanical parameters of the soil, so the Young modulus of the soil was assumed as $E = 1{\cdot}3$ MPa and the Poisson ratio as $\nu = 0{\cdot}4$, similarly as in References 26 and 36.

The calculations were performed for static air conditions (gas pressure assumed equal to

atmospheric pressure in partially saturated zone) as well as for two-phase flow. For the latter case, switching between saturated and unsaturated solutions was possible (no oscillation appeared) when $p_c = 6000$ Pa ($S \approx 0{\cdot}97$), so two-phase flow was present in a very limited zone and had only a small influence on the solution of the problem analysed. For this reason only the solution for static gas conditions is presented.

The resulting profiles of water pressure are compared with the experimental results of Liakopoulos[34] (broken curves) in Figure 1, showing their good agreement. The profiles of vertical displacements and water saturation are compared in Figure 2 with the results of Schrefler and Zhan[26] (broken curves). The transient of vertical displacements shows significant differences, although the final values of vertical displacements of the top surface are similar. The reason for the differences is the fact that we do not have the same initial conditions for displacements ($u_h(0) = u_v(0) = 0$ in the model of Schrefler and Zhan,[26] while a state of mechanical equilibrium has been imposed in the actual model). Furthermore, Schrefler and Zhan[26] used in their model the linear momentum balance equation expressed in terms of time derivatives of the primary variables. By time differentiating the equation, the set of possible solution trajectories is modified if not all initial conditions are the same in the two models, including the derivatives up to the highest order present in the ODE.

5.2. Modelling of subsidence due to pumping from a phreatic aquifer

This example deals with subsidence of saturated–unsaturated land due to pumping from an axisymmetric aquifer, which was solved previously by Safai and Pinder[37] and then by Meroi.[38] An aquifer of 10 m depth sited on an impervious layer was subjected to pumpage of 20 $m^3\ h^{-1}$ within a height of 2·5 m from the bottom. At the beginning a fully saturated state with unit vertical gradient of potential was assumed, as well as a mechanical equilibrium state.

The boundary conditions were the following: for the bottom surface, $u_v = 0$; for the top surface, $p_g = p_{atm}$; for the inner lateral surface (radius 0·3 m), an outflow of 1·179 kg s^{-1} m^{-2} within the height of 2·5 m from the bottom, $u_h = 0$; for the outer lateral surface (radius 100·3 m), full saturation of water with unit vertical gradient of potential was assumed. The temperature of the medium was assumed to be equal to 293·15 K at the beginning as well as during the whole process analysed.

The mechanical and hydraulic properties of the soil were assumed similarly as in References 37 and 38: $E = 22$ MPa, $\nu = 0{\cdot}1$, $k = 2 \times 10^{-4}$ m s^{-1}, $\phi = 0{\cdot}2$. The relationships between capillary pressure, saturation and relative permeability of water proposed by Safai and Pinder[37] were used.

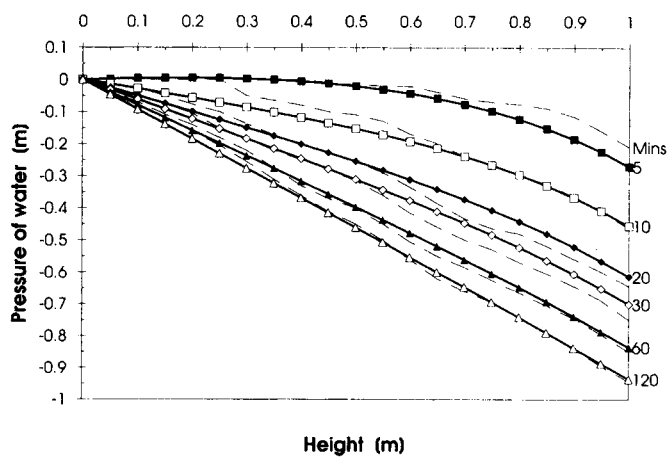

Figure 1. Comparison of numerical (full curves) and experimental results[34] (broken curves) for water pressure

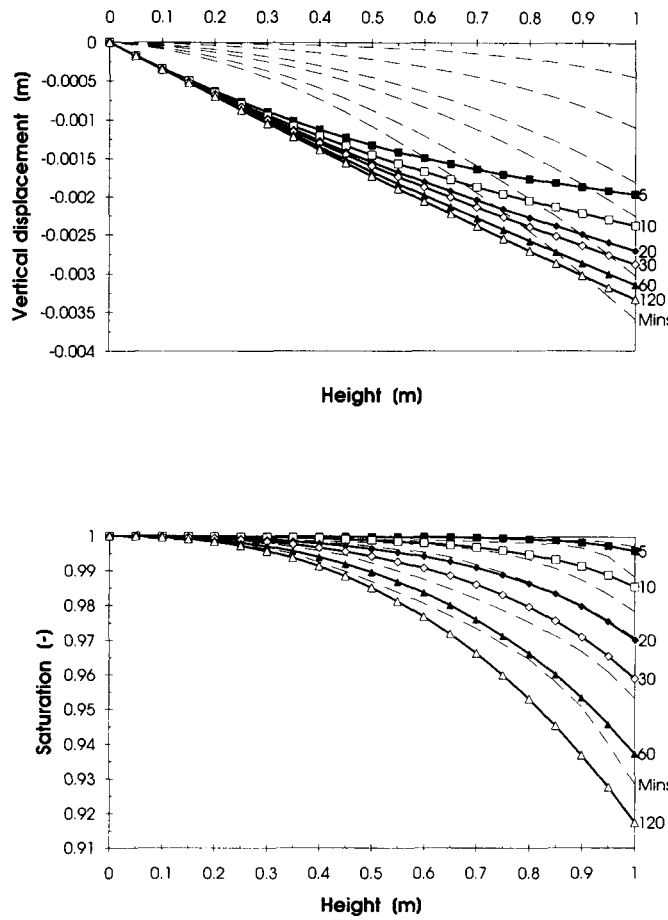

Figure 2. Resulting saturation and vertical displacement profiles (full curves) compared with solution of Schrefler and Zhan[26] (broken curves)

The relative permeability of gas proposed by Brooks and Corey[39] were applied in the partially saturated zone.

For numerical purposes the aquifer was simulated by 50 eight-node isoparametric elements (five in height and 10 in radius direction) using the same mesh as in Reference 38.

A 3 × 3 Gaussian integration scheme was applied. Temporal discretization was performed with an initial step of 1 min for the first 10 h, 10 min for the next 20 h and then 1 h until 28 days, the required time of analysis.

The resulting profiles of water saturation on the top surface of the aquifer are compared in Figure 3 with the results of Safai and Pinder[37] (broken curves), showing their relatively good agreement. It has to be mentioned that the model of Safai and Pinder neglects the fluid accumulation due to changes in the degree of saturation, which explains the differences in the early pumping phase. The profiles of water saturation on the upper surface and vertical displacements for time values of 10 min, 3, 10 and 30 h and 28 days are compared in Figure 4 with the results of Meroi[38] (broken curves). In Reference 38 the gas pressure was assumed constant and equal to atmospheric pressure in the partially saturated zone, which may explain the different time transient behaviours. Note that the final values at the centre match very well.

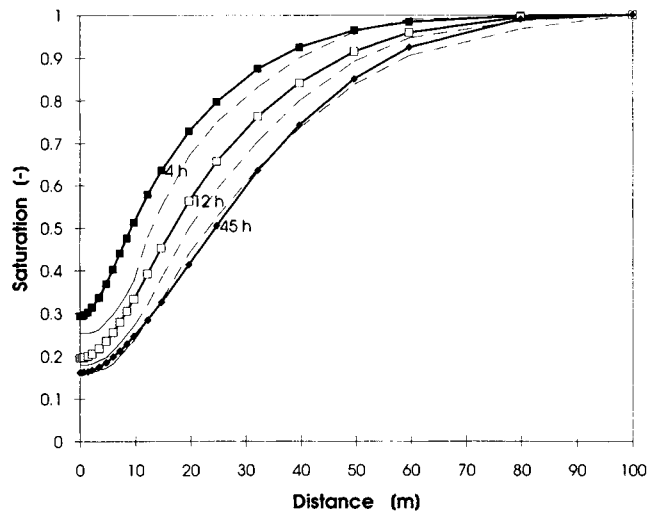

Figure 3. Resulting profiles of saturation (full curves) compared with solution of Safai and Pinder[37] (broken curves)

5.3. *Non-isothermal consolidation*

This example deals with fully and partially saturated thermoelastic consolidation, for which previous solutions are known.[13,27] In Reference 27 the fully saturated case was studied in detail, while in Reference 13 the problem was solved for the partially saturated case but neglecting latent heat and phase change. The present model takes these two factors into account and the ensuing changes in terms of displacements and especially saturations and capillary pressures in advanced stages of the simulation are of importance.

A column of 7 m height and 2 m width of linear elastic material with Young modulus $E = 6$ MPa and Poisson ratio $\nu = 0{\cdot}4$ was subjected to an external surface load of 1000 Pa and to a surface temperature jump of 50 K above the initial temperature of 293·15 K. The other data of the porous medium were assumed the same as in References 13 and 27. The relationships between capillary pressure, saturation of water and relative permeabilities of water and gas proposed by Brooks and Corey[39] were used. Water and solid phase were assumed incompressible.

The boundary conditions were the following: for the lateral surface, $q_T = 0$, $u_h = 0$; for the top surface, $T = 343{\cdot}15$ K, $\rho_g = p_{atm}$, $p_c = 0$ for the fully saturated case or $p_c = p_c^*$ for the partially saturated case, where p_c^* is the capillary pressure corresponding to saturation $S = 0{\cdot}92$; for the bottom surface, $q_T = 0$, $u_v = 0$. For numerical purposes the column was simulated by nine (the same as in Reference 27) and then by 18 eight-node isoparametric elements, giving practically the same results. 3×3 Gaussian integration scheme was used. For the fully saturated case an initial time step of 0·01 days for 10 steps was applied. This value was then multiplied by 10 and this procedure was repeated after each 10 time steps until the required time of analysis was reached. For semisaturated conditions the temporal discretization was performed with an initial step of 0·01 days during the first 100 steps and multiplied by 10 after repeating 100 steps until 10^7 days.

The problem was solved for three different cases: (i) fully saturated;[13,27] (ii) initially homogeneous saturation of water; $S = 9770{\cdot}92$,[13] and capillary pressure–saturation curve:[39] independent of temperature; (iii) initially homogeneous saturation of water, $S = 0{\cdot}92$, and modified capillary pressure–saturation relationship of Brooks and Corey[39] (assuming that it was measured at temperature $T = 293{\cdot}15$ K) with regard to the change in capillary pressure due to the dependence of surface tension on temperature.[40]

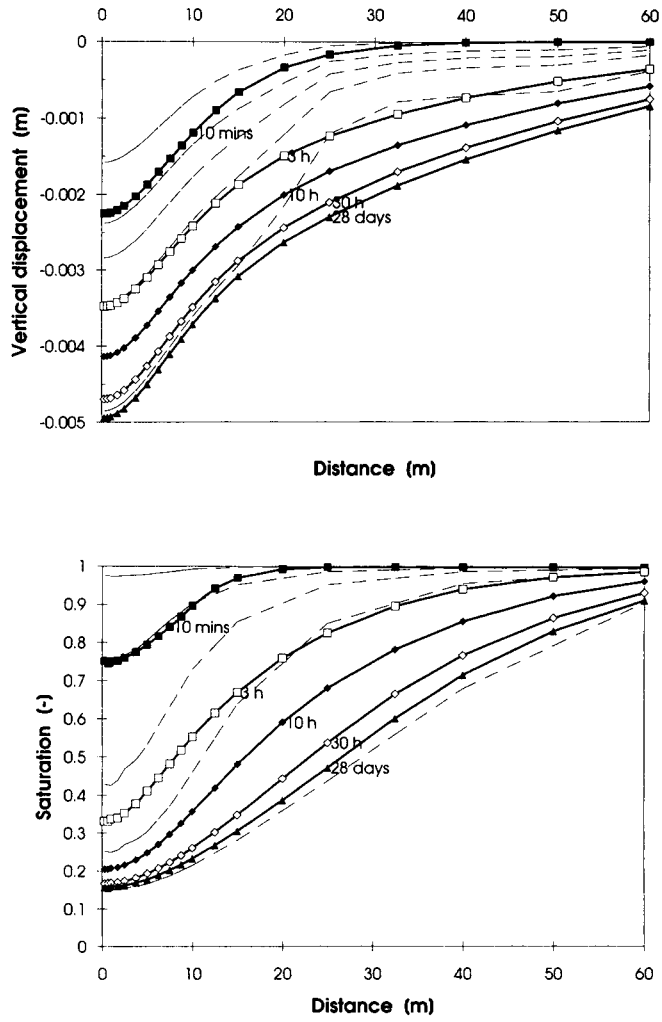

Figure 4. Resulting saturation and vertical displacement profiles (full curves) compared with solution of Meroi[38] (broken curves)

The resulting temperature profiles, practically the same for the three analysed cases (because of the assumption of the same average thermal conductivity and relatively high thermal capacity, the same as in References 13 and 27), are compared in Figure 5 with the results of Aboustit *et al.*[27] In all the figures concerning the analysed example the numbers 4, 7, 17, 27, 37 and 42 indicate some selected nodal points of the mesh used in Reference 27 which are located at 0·1, 0·2, 0·6, 1·0, 3·0 and 5·0 m from the upper surface of the column respectively. The resulting pore pressure and vertical displacement histories at several nodal points are compared in Figures 6 and 7 with the previous solutions[13,27] for the fully saturated case. In Figure 7 the settlement histories of the semisaturated medium with temperature-independent capillary pressure–saturation curve are also presented. The resulting profiles of capillary pressure and saturation of water for this case (Figure 8) show the influence of phase change on the phenomenon. The characteristic shape of the curves is an effect of previous condensation and subsequent evaporation caused by temperature changes. In the previous

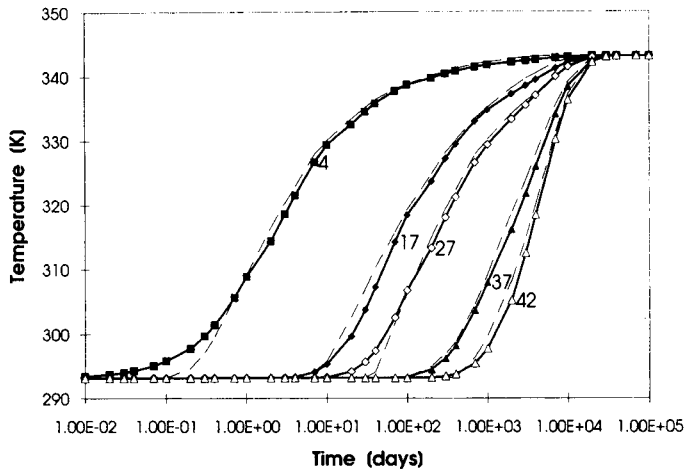

Figure 5. Resulting profiles of temperature (full curves) compared with solution of Aboustit *et al.*[27] (broken curves)

solution[13] where phase change was not taken into account this was not observed. The settlement histories of two analysed semisaturated cases are compared in Figure 9, showing the significant differences caused by the dependence of capillary pressure–saturation curve on temperature,which was omitted in Reference 13. The resulting profiles of capillary pressure and saturation of water for the third analysed case (Figure 10) show that phase change phenomena are more intensive in this case, while capillary pressure histories are strongly influenced by temperature histories, causing additional vertical displacements (Figure 9).

6. CONCLUSIONS

A fully coupled model for simulating heat and mass transfer in deformable porous media taking into account also phase change phenomena (evaporation, condensation and latent heat transfer) has been presented. The model is based on a strong physical background that allows us to clearly identify the constitutive equations and the other coefficients needed to characterize the analysed medium. The model, obtained by use of volume-averaging techniques,[1–4,9,10] results in a set of non-linear and coupled partial differential equations. These are discretized in space using the finite element method and in time using finite differences and solved for the gas pressure, capillary pressure, temperature and displacements as primary variables. Because of the non-linearity of the equations, a monolithic Newton–Raphson approach is used for solution. The validity of the approach has been demonstrated by the good agreement between simulation results and experimental data of Liakopoulos.[34] Further examples show both the robustness of the model in dealing with problems usually difficult to solve and the appreciable influence of phase change (usually neglected in other models) on the evolution of the phenomena.

ACKNOWLEDGEMENTS

This work has been carried out within the framework of the HCM project 'ALERT geomaterials'. The first author's research has been supported by the University of Padua.

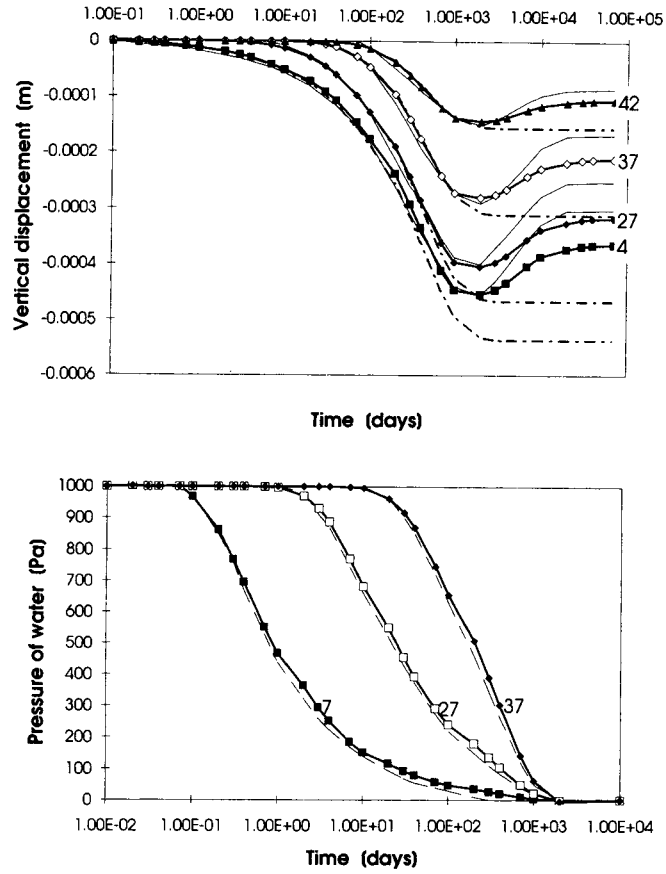

Figure 6. Resulting profiles of water pressure and vertical displacement (full curves) compared with solution of Aboustit *et al.*[27] (broken curves); chain curves indicate the isothermal solution

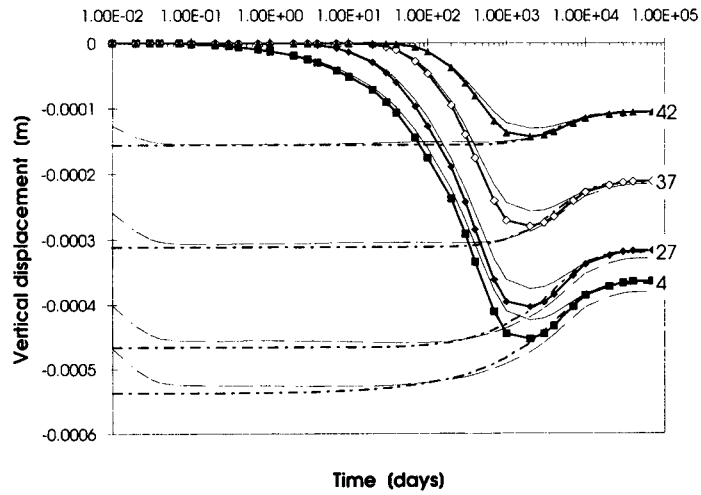

Figure 7. Comparison between saturated (full curves) and partially saturated, case (ii) solutions (chain curves); the heavy lines indicate the present solution, while fine lines indicate the solution of Schrefler *et al.*[13]

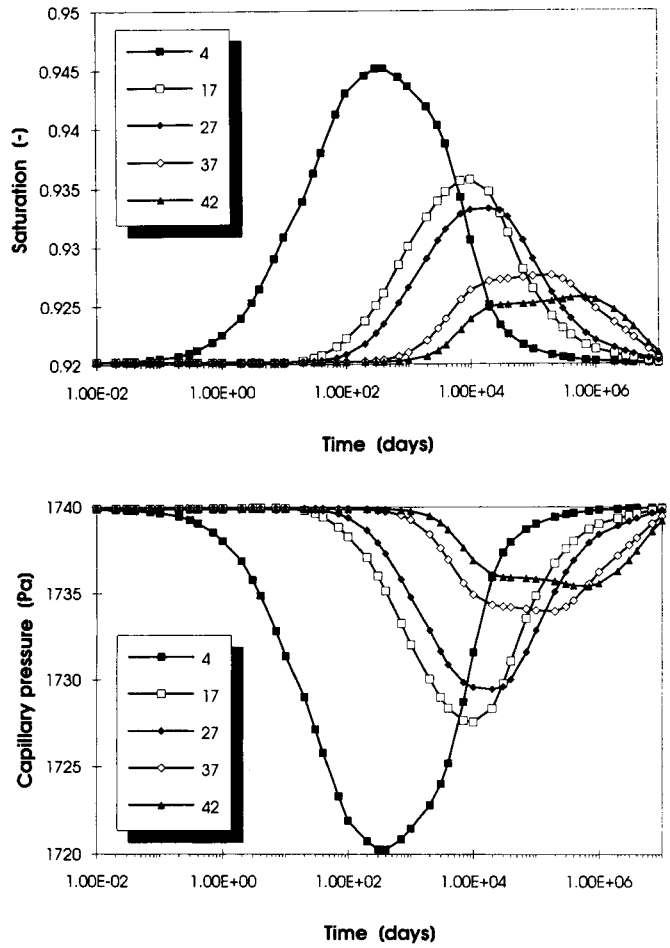

Figure 8. Resulting profiles of capillary pressure and saturation for partially saturated state, case (ii)

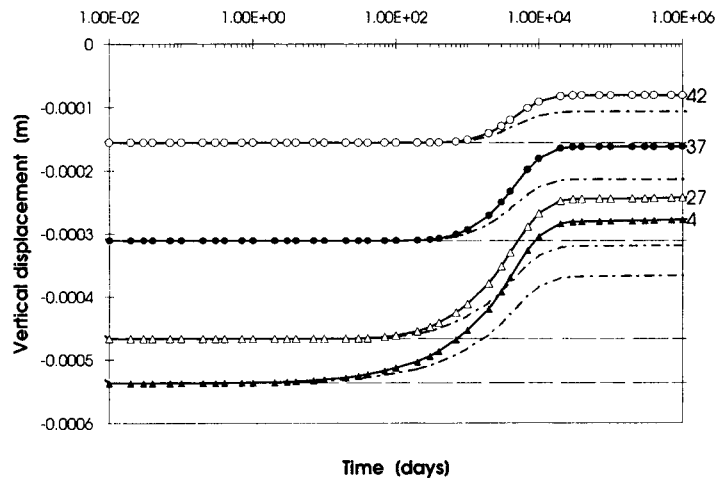

Figure 9. Comparison between solutions for partially saturated state, case (iii) (full curves) and case (ii) (chain curves); broken lines indicate the isothermal solution

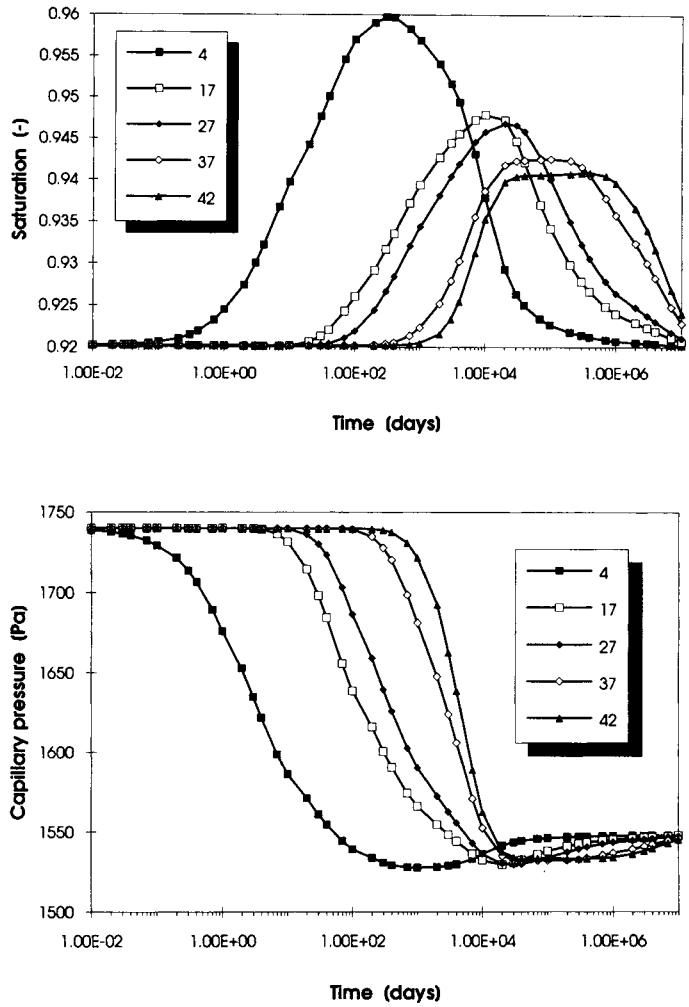

Figure 10. Resulting profiles of capillary pressure and saturation for partially saturated state, case (iii)

APPENDIX I

The governing equations (23) and (27) in the discretized form are shown here in detail using the notation of Reference 27:

$$\mathbf{K}_{gg} = -\int_{\Omega} (\nabla \mathbf{N}_p)^T \left[-\rho_{ga} \frac{KK_{rg}}{\mu_g} + \rho_g \frac{M_a M_v}{M^2} D_{eff} p_{gw} \left(\frac{-1}{p_g^2} \right) \right] \nabla \mathbf{N}_p \, d\Omega,$$

$$\mathbf{K}_{gc} = -\int_{\Omega} (\nabla \mathbf{N}_p)^T \left[\rho_g \frac{M_a M_v}{M^2} D_{eff} \frac{1}{p_g} \left(\frac{\partial p_{gw}}{\partial p_c} \right) \right] \nabla \mathbf{N}_p \, d\Omega,$$

$$\mathbf{K}_{gt} = -\int_{\Omega} (\nabla \mathbf{N}_t)^T \left[\rho_g \frac{M_a M_v}{M^2} D_{eff} \frac{1}{p_g} \left(\frac{\partial p_{gw}}{\partial T} \right) \right] \nabla \mathbf{N}_t \, d\Omega,$$

$$\mathbf{C}_{gg} = \int_\Omega \mathbf{N}_p^T \phi \left[(1-S) \left(\frac{\partial \rho_{ga}}{\partial p_g} \right) \right] \mathbf{N}_p \, d\Omega,$$

$$\mathbf{C}_{gc} = \int_\Omega \mathbf{N}_p^T \phi \left[(1-S) \left(\frac{\partial \rho_{ga}}{\partial p_c} \right) - \rho_{ga} \left(\frac{\partial S}{\partial p_c} \right) \right] \mathbf{N}_p \, d\Omega = 0,$$

$$\mathbf{C}_{gt} = \int_\Omega \mathbf{N}_t^T \phi \left[(1-S) \left(\frac{\partial \rho_{ga}}{\partial T} \right) - \rho_{ga} \left(\frac{\partial S}{\partial T} \right) \right] \mathbf{N}_t \, d\Omega,$$

$$\mathbf{C}_{gu} = \int_\Omega \mathbf{N}_p^T (1-S) \rho_{ga} \mathbf{m}^T \alpha \mathbf{B} \, d\Omega,$$

$$\mathbf{f}_g = - \int_\Gamma \mathbf{N}_p \mathbf{q}_{ga} \, d\Gamma;$$

$$\mathbf{K}_{cg} = - \int_\Omega (\nabla \mathbf{N}_p)^T \left[-\rho_{gw} \frac{KK_{rg}}{\mu_g} - \rho_g \frac{M_a M_v}{M^2} D_{eff} p_{gw} \left(-\frac{1}{p_g^2} \right) - \rho_l \frac{KK_{rl}}{\mu_l} \right] \nabla \mathbf{N}_p \, d\Omega,$$

$$\mathbf{K}_{cc} = - \int_\Omega (\nabla \mathbf{N}_p)^T \left[-\rho_g \frac{M_a M_v}{M^2} D_{eff} \frac{1}{p_g} \left(\frac{\partial p_{gw}}{\partial p_c} \right) + \rho_l \frac{KK_{rl}}{\mu_l} \right] \nabla \mathbf{N}_p \, d\Omega,$$

$$\mathbf{K}_{ct} = - \int_\Omega (\nabla \mathbf{N}_t)^T \left[-\rho_g \frac{M_a M_v}{M^2} D_{eff} \frac{1}{p_g} \left(\frac{\partial p_{gw}}{\partial T} \right) \right] \nabla \mathbf{N}_t \, d\Omega,$$

$$\mathbf{C}_{cg} = 0,$$

$$\mathbf{C}_{cc} = \int_\Omega \mathbf{N}_p^T \phi \left[(1-S) \left(\frac{\partial \rho_{gw}}{\partial p_c} \right) - \rho_{gw} \left(\frac{\partial S}{\partial p_c} \right) + \rho_l \left(\frac{\partial S}{\partial p_c} \right) \right] \mathbf{N}_p \, d\Omega = 0,$$

$$\mathbf{C}_{ct} = \int_\Omega \mathbf{N}_t^T \phi \left[(1-S) \left(\frac{\partial \rho_{gw}}{\partial T} \right) - \rho_{gw} \left(\frac{\partial S}{\partial T} \right) + \rho_l \left(\frac{\partial S}{\partial T} \right) \right] \mathbf{N}_t \, d\Omega,$$

$$\mathbf{C}_{cu} = \int_\Omega \mathbf{N}_p^T \left[(\mathbf{1}-S) \rho_{gw} + S \rho_w \right] \mathbf{m}^T \alpha \mathbf{B} \, d\Omega,$$

$$\mathbf{f}_c = - \int_\Omega (\nabla \mathbf{N}_p)^T \left(\rho_l \frac{KK_{rl}}{\mu_l} \rho_l \mathbf{b} \right) d\Omega - \int_\Gamma \mathbf{N}_p \left[\beta_c \left(\rho_{gw} - \rho_{gw\infty} \right) + q_{gw} + q_l \right] d\Gamma;$$

$$\mathbf{K}_{tg} = - \int_\Omega (\nabla \mathbf{N}_p)^T \left(\Delta h_{vap} \rho_l \frac{KK_{rl}}{\mu_l} \right) \nabla \mathbf{N}_p \, d\Omega,$$

$$\mathbf{K}_{tc} = - \int_\Omega (\nabla \mathbf{N}_p)^T \left(-\Delta h_{vap} \rho_l \frac{KK_{rl}}{\mu_l} \right) \nabla \mathbf{N}_p \, d\Omega,$$

$$\mathbf{K}_{tt} = - \int_\Omega (\nabla \mathbf{N}_t)^T \lambda_{eff} \nabla \mathbf{N}_t \, d\Omega + \int_\Omega \mathbf{N}_t^T \left(C_{pw} \rho_w \frac{KK_{rl}}{\mu_l} (\nabla p_g - \nabla p_c - \rho_l \mathbf{b}) + C_{pg} \rho_{gw} \frac{KK_{rg}}{\mu_g} \nabla p_g \right) \nabla \mathbf{N}_t \, d\Omega,$$

$$\mathbf{C}_{tg} = 0,$$

$$\mathbf{C}_{tc} = \int_\Omega \mathbf{N}_p^T \left[-\Delta h_{vap} \rho_l \phi \left(\frac{\partial S}{\partial p_c} \right) \right] \mathbf{N}_p \, d\Omega,$$

$$\mathbf{C}_{tt} = \int_\Omega \mathbf{N}_t^T \left[\rho C_p - \Delta h_{vap} \phi \rho_l \left(\frac{\partial S}{\partial T} \right) \right] \mathbf{N}_t \, d\Omega,$$

$$\mathbf{C}_{tu} = - \int_\Omega \mathbf{N}_t^T \Delta h_{vap} S \rho_w \mathbf{m}^T \alpha \mathbf{B} \, d\Omega,$$

$$\mathbf{f}_t = - \int_\Omega (\nabla \mathbf{N}_t)^T \left(-\Delta h_{vap} \rho_l \frac{K K_{rl}}{\mu_l} \rho_l \mathbf{b} \right) d\Omega - \int_\Gamma \mathbf{N}_t [\alpha_c (T - T_\infty) + q_T] d\Gamma;$$

$$\mathbf{K}_{uu} = \int_\Omega \mathbf{B}^T \mathbf{D}_T \mathbf{B} \, d\Omega,$$

$$\mathbf{K}_{ug} = \int_\Omega \mathbf{B}^T \alpha \mathbf{m} \mathbf{N}_p \, d\Omega,$$

$$\mathbf{K}_{uc} = - \int_\Omega \mathbf{B}^T \alpha S \mathbf{m} \mathbf{N}_p \, d\Omega,$$

$$\mathbf{K}_{ut} = \int_\Omega \mathbf{B}^T \mathbf{D} \frac{\beta_s}{3} \mathbf{m} \mathbf{N}_T \, d\Omega,$$

$$\mathbf{f}_u = - \int_\Omega \mathbf{N}_u \rho \mathbf{b} \, d\Omega - \int_\Gamma \mathbf{N}_u \mathbf{t} \, d\Gamma.$$

APPENDIX II: NOMENCLATURE

$\mathbf{b}$	specific body force (m s^{-2})
$\mathbf{B}$	strain matrix relating strain and displacement
C_p	effective specific heat of porous medium (J kg^{-1} K^{-1})
C_{pg}	specific heat of gas mixture (J kg^{-1} K^{-1})
C_{pl}	specific heat of liquid phase (water) (J kg^{-1} K^{-1})
C_{ps}	specific heat of solid matrix (J kg^{-1} K^{-1})
$\mathbf{D}$	tangent matrix (Pa)
D_{eff}	effective diffusivity of gas mixture (m^2 s^{-1})
E	Young modulus (Pa)
$\mathbf{I}$	unit tensor
k	hydraulic conductivity (m s^{-1})
K	absolute permeability (m^2)
K_{rg}	relative permeability of gas phase
K_{rl}	relative permeability of liquid phase
K_S	bulk modulus of solid phase
K_T	bulk modulus of porous medium
M	molar mass of gas moisture (moist air) (kg $kmol^{-1}$)
M_a	molar mass of dry air (kg $kmol^{-1}$)
M_w	molar mass of water vapour (kg $kmol^{-1}$)
$\mathbf{n}$	unit normal vector
p	average pressure of mixture (Pa)
p_{atm}	atmospheric pressure (Pa)
p_c	capillary pressure (Pa)
p_g	pressure of gas phase (Pa)
p_{gw}	water vapour partial pressure (Pa)
p_{gws}	water vapour saturation pressure (Pa)

p_l liquid water pressure (Pa)
q_{ga} dry air flux imposed on boundary
q_{gw} vapour flux imposed on boundary
q_l liquid flux imposed on boundary
q_T heat flux imposed on boundary
R gas constant (8314·41 J $kmol^{-1}$ K^{-1})
S liquid phase volumic saturation (liquid volume/pore volume)
t time (s)
$\mathbf{t}$ traction imposed on boundary (Pa)
T temperature (K)
T_∞ temperature in undisturbed gas phase far from interface (K)
$\mathbf{u}$ displacement vector of solid matrix (m)
u_h horizontal displacement (m)
u_v vertical displacement (m)
$\mathbf{v}_g$ velocity of gaseous phase (m s^{-1})
$\mathbf{v}_l$ velocity of liquid phase (m s^{-1})
$\mathbf{v}_{ga}^d$ relative average diffusion velocity of dry air species (m s^{-1})
$\mathbf{v}_{gw}^d$ relative average diffusion velocity of water vapour species (m s^{-1})

Greek letters

α Biot constant
α_c convective heat transfer coefficient (W m^{-2} K^{-1})
β_c convective mass transfer coefficient (kg m^{-3})
β_s cubic thermal expansion coefficient of solid (K^{-1})
Γ_i part of boundary Γ where value of i-variable is imposed
Γ_i^q part of boundary Γ where flux of i-variable is imposed
Δh_{vap} enthalpy of vaporization per unit mass (J kg^{-1})
Δt time step (s)
ε elastic strain
ε_v volumetric strain
ε^T thermoelastic strain
λ_{eff} effective thermal conductivity (W m^{-1} K^{-1})
μ_g gas phase dynamic viscosity (Pa s)
μ_l liquid phase dynamic viscosity (Pa s)
ν Poisson ratio
ρ effective density of porous medium (kg m^{-3})
ρ_g gas phase density (kg m^{-3})
ρ_{ga} mass concentration of dry air in gas phase (kg m^{-3})
ρ_{gw} mass concentration of water vapour in gas phase (kg m^{-3})
$\rho_{gw\infty}$ mass concentration of water vapour in undisturbed gas phase far from interface (kg m^{-3})
ρ_l liquid phase density (kg m^{-3})
σ total stress tensor (Pa)
σ'' effective stress tensor (Pa)
ϕ porosity (pore volume/total volume)

REFERENCES

1. M. Hassanizadeh and W. G. Gray, 'General conservation equations for multiphase systems: 1. Averaging technique', *Adv. Water Res.*, **2**, 131–144 (1979).
2. M. Hassanizadeh and W. G. Gray, 'General conservation equations for multiphase systems: 2. Mass, momenta, energy and entropy equations', *Adv. Water Res.*, **2**, 191–203 (1979).
3. M. Hassanizadeh and W. G. Gray, 'General conservtion equations for multiphase systems: 3. Constitutive theory for porous media flow', *Adv. Water Res.*, **3**, 25–40 (1980).
4. J. Bear, *Dynamics of Fluids in Porous Media*, Dover, New York, 1988.
5. J. Bear, *Hydraulics of Groundwater*, McGraw-Hill, New York, 1979.
6. J. Bear and Y. Bachmat, *Introduction to Modeling of Transport Phenomena in Porous Media*, Kluwer, Dordrecht, 1990.
7. Y. Bachmat and J. Bear, 'Macroscopic modelling of transport phenomena in porous media. 1: The continuum approach', *J. Transp. Porous Media*, **1**, 213–240 (1986).

8. Y. Bachmat and J Bear, 'Macroscopic modelling of transport phenomena in porous media. 2: Applications to mass momentum and energy transfer', *J. Transp. Porous Media*, **1**, 241–269 (1986).
9. S. Whitaker, 'Simultaneous heat, mass and momentum transfer in porous media: a theory of drying', in *Advances in Heat Transfer*, Vol. 13, Academic, New York, 1977.
10. S. Whitaker, 'Heat and mass transfer in granular porous media', in *Advances in Drying*, Vol. 1, Hemisphere, New York, 1980.
11. P. Baggio, C. E. Majorana and B. A. Schrefler, 'Hydrothermomechanical analysis of concrete by a finite element method', in R. W. Lewis (ed.), *Proc. 8th Int. Conf. on Numerical Methods for Thermal Problems*, Pineridge, Swansea, 1993, pp. 847–859.
12. P. Baggio, C. Bonacina and M. Strada, 'Trasporto di calore e di massa nel calcestruzzo celulare', *La Termotecnica*, **45**, (12), 53–60 (1993).
13. B. A. Schrefler, X. Zhan and L. Simoni, 'A coupled model for water flow, airflow and heat flow in deformable porous media', *Int. J. Numer. Methods Heat Fluid Flow*, in press.
14. V. Dakshanamurthy and D. G. Frelund, 'A mathematical model for predicting moisture flow in an unsaturated soil under hydraulic and temperature gradients', *Water Resources Res.*, **17**, 714–722 (1981).
15. H. Thomas, 'Modelling two-dimensional heat and moisture transfer in unsaturated soils, including gravity effects', *Int. J. Numer. Anal. Methods Geomech.*, **9**, 573–588 (1985).
16. H. R. Thomas and S. D. King, 'Coupled temperature/capillary potential variation in unsaturated soils', *J. Eng. Mech.*, **117**, 2475–2490 (1991).
17. M. Geraminegad and S. K. Saxena, 'A coupled thermoelastic model for saturated–unsaturated porous media', *Geotechnique*, **36**, 539–550 (1986).
18. R. W. Lewis, P. J. Roberts and B. A. Schrefler, 'Finite element modelling of two phase heat and fluid flow in deforming porous media', *J. Transp. Porous Media*, **4**, 319–334 (1989).
19. J. R. Philip and D. A. De Vries, 'Moisture movements in porous material under temperature gradients', *Trans. Am. Geophys. Union*, **38**, 222–232 (1957).
20. D. A. De Vries, 'Simultaneous transfer of heat and moisture in porous media', *Trans. Am. Geophys. Union*, **39**, 909–916 (1958).
21. Hyland and Wexler, *ASHRAE Handbook, Fundamentals Volume*, ASHRAE, Atlanta, GA, 1993.
22. S. Whitaker, 'The transport equations for multiphase systems', *Chem. Eng. Sci.*, **28**, 139–147 (1973).
23. M. A. Biot and P. G. Willis, 'The elastic coefficients of the theory of consolidation', *J. Appl. Mech.*, **24**, 594–601 (1957).
24. A. W. Skempton, 'Effective stress in soils, concrete and rocks', in *Pore Pressure and Suction in Soil*, Gutterworth, Stoneham, MA, 1961, pp. 4–16.
25. O. C. Zienkiewicz, Y. M. Xie, B. A. Schrefler, A. Ledesma and N. Bicanic, 'Static and dynamic behaviour of soils: a rational approach to quantitative solutions, II, Semisaturated problems', *Proc. R. Soc. Lond. A*, **429**, 311–321 (1990).
26. B. A. Schrefler and X. Zhan, 'A fully coupled model for water flow and airflow in deformable porous media', *Water Resources Res.*, **29**, 155–167 (1993).
27. R. W. Lewis and B. A. Schrefler, *The Finite Element Method in the Deformation and Consolidation of Porous Media*, Wiley, New York, 1987.
28. P. Baggio and C. Bonacina, 'Introduction to modeling heat and mass transfer in porous building material', *Q. Ist. Fis. Tec. Univ. Padova*, **146**, in press (in Italian).
29. B. A. Schrefler, L. Simoni, X. Li and O. C. Zienkiewicz, 'Mechanics of partially saturated porous media', in C. S. Desai and G. Gioda (eds), *CISM Courses and Lectures*, Vol. 311, *Numerical Methods and Constitutive Modelling in Geomechanics*, Springer, New York, 1990, pp. 169–209.
30. O. Coussy, *Mecanique des Milieux Poreux*, Editions Technip, Paris, 1991.
31. R. de Boer, W. Ehlers, S. Kowalski and J. Plischka, *Porous Media, a Survey of Different Approaches*, Fachbereich Bauwesen der Universität Gesamthochschule, Essen, 1991, Heft 54.
32. O. C. Zienkiewicz and R. L. Taylor, *The Finite Element Method*, Vols 1 and 2, 4th edn, McGraw Hill, London, 1989 and 1991.
33. P. A. Forsyth and R. B. Simpson, 'A two-phase, two-component model for natural convection in a porous medium', *Int. J. Numer. Methods Fluids*, **12**, 655–682 (1991).
34. A. C. Liakopoulos, 'Transient flow through unsaturated porous media', *Ph.D. Thesis*, University of California, Berkeley, CA, 1965.
35. T. N. Narasimhan and P. A. Witherspoon, 'Numerical model for saturated–unsaturated flow in deformable porous media. 3. Applications', *Water Resource Res.*, **14**, 1017–1034 (1978).
36. B. A. Schrefler and L. Simoni, 'A unified approach to the analysis of saturated–unsaturated elastoplastic porous media', in G. Svoboda (ed.), *Numerical Methods in Geomechanics*, Balkema, Rotterdam, 1988, pp. 205–212.
37. N. M. Safai and G. F. Pinder, 'Vertical and horizontal land deformation in a desaturating porous medium', *Adv. Water Resources*, **2**, 19–25 (1979).
38. E. Meroi, 'Comportamento non lineare per geometria di mezzi porosi parzialmente saturi', *Tesi di Dottorato in Meccanica delle Strutture*, Facolta di Ingegneria, Universitá di Padova, 1993.
39. R. N. Brooks and A. T. Corey, 'Properties of porous media affecting fluid flow', *J. Irrig. Drain. Div. Am. Soc. Civil Eng.*, **92** (IR2), 61–68 (1966).
40. O. Krischer and K. Kroell, *Trocknungstechnik*, Band 1, *Die Wissenschaftlichen Grundlagen der Trocknungstechnik*, 3. Aufl., Springer, Berlin, 1978.